

# Measurement of elliptic flow of $J/\psi$ in $\sqrt{s_{NN}} = 200$ GeV Au+Au collisions at forward rapidity

N.J. Abdulameer,<sup>15,22</sup> U. Acharya,<sup>19</sup> A. Adare,<sup>12</sup> C. Aidala,<sup>42</sup> N.N. Ajitanand,<sup>61,\*</sup> Y. Akiba,<sup>56,57,†</sup> M. Alfred,<sup>21</sup> S. Antsupov,<sup>59</sup> K. Aoki,<sup>31,56</sup> N. Apadula,<sup>27,62</sup> H. Asano,<sup>34,56</sup> C. Ayuso,<sup>42</sup> B. Azmoun,<sup>7</sup> V. Babintsev,<sup>23</sup> M. Bai,<sup>6</sup> N.S. Bandara,<sup>40</sup> B. Bannier,<sup>62</sup> E. Bannikov,<sup>59</sup> K.N. Barish,<sup>8</sup> S. Bathe,<sup>5,57</sup> A. Bazilevsky,<sup>7</sup> M. Beaumier,<sup>8</sup> S. Beckman,<sup>12</sup> R. Belmont,<sup>12,49</sup> A. Berdnikov,<sup>59</sup> Y. Berdnikov,<sup>59</sup> L. Bichon,<sup>67</sup> B. Blankenship,<sup>67</sup> D.S. Blau,<sup>33,46</sup> M. Boer,<sup>36</sup> J.S. Bok,<sup>48</sup> V. Borisov,<sup>59</sup> K. Boyle,<sup>57</sup> M.L. Brooks,<sup>36</sup> J. Bryslawskyj,<sup>5,8</sup> V. Bumazhnov,<sup>23</sup> C. Butler,<sup>19</sup> S. Campbell,<sup>13,27</sup> V. Canoa Roman,<sup>62</sup> C.-H. Chen,<sup>57</sup> D. Chen,<sup>62</sup> M. Chiu,<sup>7</sup> C.Y. Chi,<sup>13</sup> I.J. Choi,<sup>24</sup> J.B. Choi,<sup>29,\*</sup> T. Chujo,<sup>65</sup> Z. Citron,<sup>68</sup> M. Connors,<sup>19,57</sup> R. Corliss,<sup>62</sup> M. Csanád,<sup>16</sup> T. Csörgő,<sup>41,69</sup> L. D. Liu,<sup>53</sup> T.W. Danley,<sup>50</sup> A. Datta,<sup>47</sup> M.S. Daugherty,<sup>1</sup> G. David,<sup>7,62</sup> K. DeBlasio,<sup>47</sup> K. Dehmelt,<sup>62</sup> A. Denisov,<sup>23</sup> A. Deshpande,<sup>57,62</sup> E.J. Desmond,<sup>7</sup> A. Dion,<sup>62</sup> P.B. Diss,<sup>39</sup> V. Doomra,<sup>62</sup> J.H. Do,<sup>70</sup> A. Drees,<sup>62</sup> K.A. Drees,<sup>6</sup> M. Dumancic,<sup>68</sup> J.M. Durham,<sup>36</sup> A. Durum,<sup>23</sup> T. Elder,<sup>19</sup> A. Enokizono,<sup>56,58</sup> R. Esha,<sup>62</sup> B. Fadem,<sup>44</sup> W. Fan,<sup>62</sup> N. Feege,<sup>62</sup> D.E. Fields,<sup>47</sup> M. Finger, Jr.,<sup>9</sup> M. Finger,<sup>9</sup> D. Firak,<sup>15,62</sup> D. Fitzgerald,<sup>42</sup> S.L. Fokin,<sup>33</sup> J.E. Frantz,<sup>50</sup> A. Franz,<sup>7</sup> A.D. Frawley,<sup>18</sup> Y. Fukuda,<sup>65</sup> P. Gallus,<sup>14</sup> C. Gal,<sup>62</sup> P. Garg,<sup>3,62</sup> H. Ge,<sup>62</sup> F. Giordano,<sup>24</sup> A. Glenn,<sup>35</sup> Y. Goto,<sup>56,57</sup> N. Grau,<sup>2</sup> S.V. Greene,<sup>67</sup> M. Grosse Perdekamp,<sup>24</sup> T. Gunji,<sup>11</sup> T. Guo,<sup>62</sup> T. Hachiya,<sup>56,57</sup> J.S. Haggerty,<sup>7</sup> K.I. Hahn,<sup>17</sup> H. Hamagaki,<sup>11</sup> H.F. Hamilton,<sup>1</sup> J. Hanks,<sup>62</sup> S.Y. Han,<sup>17,32</sup> S. Hasegawa,<sup>28</sup> T.O.S. Haseler,<sup>19</sup> K. Hashimoto,<sup>56,58</sup> T.K. Hemmick,<sup>62</sup> X. He,<sup>19</sup> J.C. Hill,<sup>27</sup> K. Hill,<sup>12</sup> A. Hodges,<sup>19,24</sup> R.S. Hollis,<sup>8</sup> K. Homma,<sup>20</sup> B. Hong,<sup>32</sup> T. Hoshino,<sup>20</sup> N. Hotvedt,<sup>27</sup> J. Huang,<sup>7</sup> K. Imai,<sup>28</sup> J. Imrek,<sup>15</sup> M. Inaba,<sup>65</sup> A. Iordanova,<sup>8</sup> D. Isenhower,<sup>1</sup> Y. Ito,<sup>45</sup> D. Ivanishchev,<sup>55</sup> B. Jacak,<sup>62</sup> M. Jezghani,<sup>19</sup> X. Jiang,<sup>36</sup> Z. Ji,<sup>62</sup> B.M. Johnson,<sup>7,19</sup> V. Jorjadze,<sup>62</sup> D. Jouan,<sup>52</sup> D.S. Jumper,<sup>24</sup> S. Kanda,<sup>11</sup> J.H. Kang,<sup>70</sup> D. Kapukchyan,<sup>8</sup> S. Karthas,<sup>62</sup> D. Kawall,<sup>40</sup> A.V. Kazantsev,<sup>33</sup> J.A. Key,<sup>47</sup> V. Khachatryan,<sup>62</sup> A. Khanzadeev,<sup>55</sup> B. Kimelman,<sup>44</sup> C. Kim,<sup>8,32</sup> D.J. Kim,<sup>30</sup> E.-J. Kim,<sup>29</sup> G.W. Kim,<sup>17</sup> M. Kim,<sup>60</sup> M.H. Kim,<sup>32</sup> D. Kincses,<sup>16</sup> E. Kistenev,<sup>7</sup> R. Kitamura,<sup>11</sup> J. Klatsky,<sup>18</sup> D. Kleinjan,<sup>8</sup> P. Kline,<sup>62</sup> T. Koblesky,<sup>12</sup> B. Komkov,<sup>55</sup> D. Kotov,<sup>55,59</sup> L. Kovacs,<sup>16</sup> S. Kudo,<sup>65</sup> K. Kurita,<sup>58</sup> M. Kurosawa,<sup>56,57</sup> Y. Kwon,<sup>70</sup> J.G. Lajoie,<sup>27,51</sup> E.O. Lallow,<sup>44</sup> A. Lebedev,<sup>27</sup> S. Lee,<sup>70</sup> S.H. Lee,<sup>27,62</sup> M.J. Leitch,<sup>36</sup> Y.H. Leung,<sup>62</sup> N.A. Lewis,<sup>42</sup> S.H. Lim,<sup>36,54,70</sup> M.X. Liu,<sup>36</sup> X. Li,<sup>10</sup> X. Li,<sup>36</sup> V.-R. Loggins,<sup>24</sup> S. Lökös,<sup>69</sup> D.A. Loomis,<sup>42</sup> D. Lynch,<sup>7</sup> T. Majoros,<sup>15</sup> Y.I. Makdisi,<sup>6</sup> M. Makek,<sup>71</sup> M. Malaev,<sup>55</sup> A. Manion,<sup>62</sup> V.I. Manko,<sup>33</sup> E. Mannel,<sup>7</sup> H. Masuda,<sup>58</sup> M. McCumber,<sup>36</sup> P.L. McGaughey,<sup>36</sup> D. McGlinchey,<sup>12,36</sup> C. McKinney,<sup>24</sup> A. Meles,<sup>48</sup> M. Mendoza,<sup>8</sup> A.C. Mignerey,<sup>39</sup> D.E. Mihalik,<sup>62</sup> A. Milov,<sup>68</sup> D.K. Mishra,<sup>4</sup> J.T. Mitchell,<sup>7</sup> M. Mitranskova,<sup>59,62</sup> Iu. Mitrankov,<sup>59,62</sup> G. Mitsuka,<sup>31,57</sup> S. Miyasaka,<sup>56,64</sup> S. Mizuno,<sup>56,65</sup> A.K. Mohanty,<sup>4</sup> P. Montuenga,<sup>24</sup> T. Moon,<sup>32,70</sup> D.P. Morrison,<sup>7</sup> S.I. Morrow,<sup>67</sup> T.V. Moukhanova,<sup>33</sup> B. Mulilo,<sup>32,56,72</sup> T. Murakami,<sup>34,56</sup> J. Murata,<sup>56,58</sup> A. Mwai,<sup>61</sup> K. Nagai,<sup>64</sup> K. Nagashima,<sup>20</sup> T. Nagashima,<sup>58</sup> J.L. Nagle,<sup>12</sup> M.I. Nagy,<sup>16</sup> I. Nakagawa,<sup>56,57</sup> H. Nakagomi,<sup>56,65</sup> K. Nakano,<sup>56,64</sup> C. Nattrass,<sup>63</sup> P.K. Netrakanti,<sup>4</sup> T. Niida,<sup>65</sup> S. Nishimura,<sup>11</sup> R. Nouicer,<sup>7,57</sup> N. Novitzky,<sup>30,62</sup> R. Novotny,<sup>14</sup> T. Novák,<sup>41,69</sup> G. Nukazuka,<sup>56,57</sup> A.S. Nyanin,<sup>33</sup> E. O'Brien,<sup>7</sup> C.A. Ogilvie,<sup>27</sup> J.D. Orjuela Koop,<sup>12</sup> M. Orosz,<sup>15,22</sup> J.D. Osborn,<sup>42,51</sup> A. Oskarsson,<sup>37</sup> K. Ozawa,<sup>31,65</sup> R. Pak,<sup>7</sup> V. Pantuev,<sup>25</sup> V. Papavassiliou,<sup>48</sup> J.S. Park,<sup>60</sup> S. Park,<sup>43,56,60,62</sup> M. Patel,<sup>27</sup> S.F. Pate,<sup>48</sup> J.-C. Peng,<sup>24</sup> W. Peng,<sup>67</sup> D.V. Perepelitsa,<sup>7,12</sup> G.D.N. Perera,<sup>48</sup> D.Yu. Peressounko,<sup>33</sup> C.E. PerezLara,<sup>62</sup> J. Perry,<sup>27</sup> R. Petti,<sup>7,62</sup> M. Phipps,<sup>7,24</sup> C. Pinkenburg,<sup>7</sup> R. Pinson,<sup>1</sup> R.P. Pisani,<sup>7</sup> M. Potekhin,<sup>7</sup> A. Pun,<sup>50</sup> M.L. Purschke,<sup>7</sup> J. Rak,<sup>30</sup> B.J. Ramson,<sup>42</sup> I. Ravinovich,<sup>68</sup> K.F. Read,<sup>51,63</sup> D. Reynolds,<sup>61</sup> V. Riabov,<sup>46,55</sup> Y. Riabov,<sup>55,59</sup> D. Richford,<sup>5,66</sup> T. Rinn,<sup>27</sup> S.D. Rolnick,<sup>8</sup> M. Rosati,<sup>27</sup> Z. Rowan,<sup>5</sup> J.G. Rubin,<sup>42</sup> J. Runchey,<sup>27</sup> B. Sahlmueller,<sup>62</sup> N. Saito,<sup>31</sup> T. Sakaguchi,<sup>7</sup> H. Sako,<sup>28</sup> V. Samsonov,<sup>46,55</sup> M. Sarsour,<sup>19</sup> K. Sato,<sup>65</sup> S. Sato,<sup>28</sup> B. Schaefer,<sup>67</sup> B.K. Schmoll,<sup>63</sup> K. Sedgwick,<sup>8</sup> R. Seidl,<sup>56,57</sup> A. Seleznev,<sup>59</sup> A. Sen,<sup>27,63</sup> R. Seto,<sup>8</sup> P. Sett,<sup>4</sup> A. Sexton,<sup>39</sup> D. Sharma,<sup>62</sup> I. Shein,<sup>23</sup> Z. Shi,<sup>36</sup> T.-A. Shibata,<sup>56,64</sup> K. Shigaki,<sup>20</sup> M. Shimomura,<sup>27,45</sup> P. Shukla,<sup>4</sup> A. Sickles,<sup>7,24</sup> C.L. Silva,<sup>36</sup> D. Silvermyr,<sup>37,51</sup> B.K. Singh,<sup>3</sup> C.P. Singh,<sup>3,\*</sup> V. Singh,<sup>3</sup> M. Slunečka,<sup>9</sup> K.L. Smith,<sup>18,36</sup> M. Snowball,<sup>36</sup> R.A. Soltz,<sup>35</sup> W.E. Sondheim,<sup>36</sup> S.P. Sorensen,<sup>63</sup> I.V. Sourikova,<sup>7</sup> P.W. Stankus,<sup>51</sup> M. Stepanov,<sup>40,\*</sup> S.P. Stoll,<sup>7</sup> T. Sugitate,<sup>20</sup> A. Sukhanov,<sup>7</sup> T. Sumita,<sup>56</sup> J. Sun,<sup>62</sup> Z. Sun,<sup>15,22,62</sup> S. Syed,<sup>19</sup> J. Sziklai,<sup>69</sup> A. Takeda,<sup>45</sup> A. Taketani,<sup>56,57</sup> K. Tanida,<sup>28,57,60</sup> M.J. Tannenbaum,<sup>7</sup> S. Tarafdar,<sup>67,68</sup> A. Taranenko,<sup>46,61</sup> G. Tarnai,<sup>15</sup> R. Tieulent,<sup>19,38</sup> A. Timilsina,<sup>27</sup> T. Todoroki,<sup>56,57,65</sup> M. Tomášek,<sup>14</sup> C.L. Towell,<sup>1</sup> R. Towell,<sup>1</sup> R.S. Towell,<sup>1</sup> I. Tserruya,<sup>68</sup> Y. Ueda,<sup>20</sup> B. Ujvari,<sup>15,22</sup> H.W. van Hecke,<sup>36</sup> S. Vazquez-Carson,<sup>12</sup> J. Velkovska,<sup>67</sup> M. Virius,<sup>14</sup> V. Vrba,<sup>14,26</sup> X.R. Wang,<sup>48,57</sup> Z. Wang,<sup>5</sup> Y. Watanabe,<sup>56,57</sup> Y.S. Watanabe,<sup>11,31</sup> F. Wei,<sup>48</sup> A.S. White,<sup>42</sup> C.P. Wong,<sup>7,19,36</sup> C.L. Woody,<sup>7</sup> M. Wysocki,<sup>51</sup> B. Xia,<sup>50</sup> L. Xue,<sup>19</sup> C. Xu,<sup>48</sup> Q. Xu,<sup>67</sup> S. Yalcin,<sup>62</sup> Y.L. Yamaguchi,<sup>11,57,62</sup> A. Yanovich,<sup>23</sup> P. Yin,<sup>12</sup> I. Yoon,<sup>60</sup> J.H. Yoo,<sup>32</sup> I.E. Yushmanov,<sup>33</sup> H. Yu,<sup>48,53</sup> W.A. Zajc,<sup>13</sup> A. Zelenski,<sup>6</sup> S. Zhou,<sup>10</sup> and L. Zou<sup>8</sup>

## (PHENIX Collaboration)

- <sup>1</sup>Abilene Christian University, Abilene, Texas 79699, USA
- <sup>2</sup>Department of Physics, Augustana University, Sioux Falls, South Dakota 57197, USA
- <sup>3</sup>Department of Physics, Banaras Hindu University, Varanasi 221005, India
- <sup>4</sup>Bhabha Atomic Research Centre, Bombay 400 085, India
- <sup>5</sup>Baruch College, City University of New York, New York, New York, 10010 USA
- <sup>6</sup>Collider-Accelerator Department, Brookhaven National Laboratory, Upton, New York 11973-5000, USA
- <sup>7</sup>Physics Department, Brookhaven National Laboratory, Upton, New York 11973-5000, USA
- <sup>8</sup>University of California-Riverside, Riverside, California 92521, USA
- <sup>9</sup>Charles University, Faculty of Mathematics and Physics, 180 00 Troja, Prague, Czech Republic
- <sup>10</sup>Science and Technology on Nuclear Data Laboratory, China Institute of Atomic Energy, Beijing 102413, People's Republic of China
- <sup>11</sup>Center for Nuclear Study, Graduate School of Science, University of Tokyo, 7-3-1 Hongo, Bunkyo, Tokyo 113-0033, Japan
- <sup>12</sup>University of Colorado, Boulder, Colorado 80309, USA
- <sup>13</sup>Columbia University, New York, New York 10027 and Nevis Laboratories, Irvington, New York 10533, USA
- <sup>14</sup>Czech Technical University, Zikova 4, 166 36 Prague 6, Czech Republic
- <sup>15</sup>Debrecen University, H-4010 Debrecen, Egyetem tér 1, Hungary
- <sup>16</sup>ELTE, Eötvös Loránd University, H-1117 Budapest, Pázmány P. s. 1/A, Hungary
- <sup>17</sup>Ewha Womans University, Seoul 120-750, Korea
- <sup>18</sup>Florida State University, Tallahassee, Florida 32306, USA
- <sup>19</sup>Georgia State University, Atlanta, Georgia 30303, USA
- <sup>20</sup>Physics Program and International Institute for Sustainability with Knotted Chiral Meta Matter (SKCM2), Hiroshima University, Higashi-Hiroshima, Hiroshima 739-8526, Japan
- <sup>21</sup>Department of Physics and Astronomy, Howard University, Washington, DC 20059, USA
- <sup>22</sup>HUN-REN ATOMKI, H-4026 Debrecen, Bem tér 18/c, Hungary
- <sup>23</sup>IHEP Protvino, State Research Center of Russian Federation, Institute for High Energy Physics, Protvino, 142281, Russia
- <sup>24</sup>University of Illinois at Urbana-Champaign, Urbana, Illinois 61801, USA
- <sup>25</sup>Institute for Nuclear Research of the Russian Academy of Sciences, prospekt 60-letiya Oktyabrya 7a, Moscow 117312, Russia
- <sup>26</sup>Institute of Physics, Academy of Sciences of the Czech Republic, Na Slovance 2, 182 21 Prague 8, Czech Republic
- <sup>27</sup>Iowa State University, Ames, Iowa 50011, USA
- <sup>28</sup>Advanced Science Research Center, Japan Atomic Energy Agency, 2-4 Shirakata Shirane, Tokai-mura, Naka-gun, Ibaraki-ken 319-1195, Japan
- <sup>29</sup>Jeonbuk National University, Jeonju, 54896, Korea
- <sup>30</sup>Helsinki Institute of Physics and University of Jyväskylä, P.O.Box 35, FI-40014 Jyväskylä, Finland
- <sup>31</sup>KEK, High Energy Accelerator Research Organization, Tsukuba, Ibaraki 305-0801, Japan
- <sup>32</sup>Korea University, Seoul 02841, Korea
- <sup>33</sup>National Research Center "Kurchatov Institute", Moscow, 123098 Russia
- <sup>34</sup>Kyoto University, Kyoto 606-8502, Japan
- <sup>35</sup>Lawrence Livermore National Laboratory, Livermore, California 94550, USA
- <sup>36</sup>Los Alamos National Laboratory, Los Alamos, New Mexico 87545, USA
- <sup>37</sup>Department of Physics, Lund University, Box 118, SE-221 00 Lund, Sweden
- <sup>38</sup>IPNL, CNRS/IN2P3, Univ Lyon, Université Lyon 1, F-69622, Villeurbanne, France
- <sup>39</sup>University of Maryland, College Park, Maryland 20742, USA
- <sup>40</sup>Department of Physics, University of Massachusetts, Amherst, Massachusetts 01003-9337, USA
- <sup>41</sup>MATE, Laboratory of Femtoscopy, Károly Róbert Campus, H-3200 Gyöngyös, Mátrai út 36, Hungary
- <sup>42</sup>Department of Physics, University of Michigan, Ann Arbor, Michigan 48109-1040, USA
- <sup>43</sup>Mississippi State University, Mississippi State, Mississippi 39762, USA
- <sup>44</sup>Muhlenberg College, Allentown, Pennsylvania 18104-5586, USA
- <sup>45</sup>Nara Women's University, Kita-uoya Nishi-machi Nara 630-8506, Japan
- <sup>46</sup>National Research Nuclear University, MEPhI, Moscow Engineering Physics Institute, Moscow, 115409, Russia
- <sup>47</sup>University of New Mexico, Albuquerque, New Mexico 87131, USA
- <sup>48</sup>New Mexico State University, Las Cruces, New Mexico 88003, USA
- <sup>49</sup>Physics and Astronomy Department, University of North Carolina at Greensboro, Greensboro, North Carolina 27412, USA
- <sup>50</sup>Department of Physics and Astronomy, Ohio University, Athens, Ohio 45701, USA
- <sup>51</sup>Oak Ridge National Laboratory, Oak Ridge, Tennessee 37831, USA
- <sup>52</sup>IPN-Orsay, Univ. Paris-Sud, CNRS/IN2P3, Université Paris-Saclay, BPI, F-91406, Orsay, France
- <sup>53</sup>Peking University, Beijing 100871, People's Republic of China
- <sup>54</sup>Pusan National University, Pusan 46241, Korea
- <sup>55</sup>PNPI, Petersburg Nuclear Physics Institute, Gatchina, Leningrad region, 188300, Russia
- <sup>56</sup>RIKEN Nishina Center for Accelerator-Based Science, Wako, Saitama 351-0198, Japan
- <sup>57</sup>RIKEN BNL Research Center, Brookhaven National Laboratory, Upton, New York 11973-5000, USA
- <sup>58</sup>Physics Department, Rikkyo University, 3-34-1 Nishi-Ikebukuro, Toshima, Tokyo 171-8501, Japan
- <sup>59</sup>Saint Petersburg State Polytechnic University, St. Petersburg, 195251 Russia

<sup>60</sup>Department of Physics and Astronomy, Seoul National University, Seoul 151-742, Korea

<sup>61</sup>Chemistry Department, Stony Brook University, SUNY, Stony Brook, New York 11794-3400, USA

<sup>62</sup>Department of Physics and Astronomy, Stony Brook University, SUNY, Stony Brook, New York 11794-3800, USA

<sup>63</sup>University of Tennessee, Knoxville, Tennessee 37996, USA

<sup>64</sup>Department of Physics, Tokyo Institute of Technology, Oh-okayama, Meguro, Tokyo 152-8551, Japan

<sup>65</sup>Tomonaga Center for the History of the Universe, University of Tsukuba, Tsukuba, Ibaraki 305, Japan

<sup>66</sup>United States Merchant Marine Academy, Kings Point, New York 11024, USA

<sup>67</sup>Vanderbilt University, Nashville, Tennessee 37235, USA

<sup>68</sup>Weizmann Institute, Rehovot 76100, Israel

<sup>69</sup>Institute for Particle and Nuclear Physics, HUN-REN Wigner Research Centre for Physics, (HUN-REN Wigner RCP, RMI), H-1525 Budapest 114, POBox 49, Budapest, Hungary

<sup>70</sup>Yonsei University, IPAP, Seoul 120-749, Korea

<sup>71</sup>Department of Physics, Faculty of Science, University of Zagreb, Bijenička c. 32 HR-10002 Zagreb, Croatia

<sup>72</sup>Department of Physics, School of Natural Sciences, University of Zambia, Great East Road Campus, Box 32379, Lusaka, Zambia

(Dated: September 20, 2024)

We report the first measurement of the azimuthal anisotropy of  $J/\psi$  at forward rapidity ( $1.2 < |\eta| < 2.2$ ) in Au+Au collisions at  $\sqrt{s_{NN}} = 200$  GeV at the Relativistic Heavy Ion Collider. The data were collected by the PHENIX experiment in 2014 and 2016 with integrated luminosity of  $14.5 \text{ nb}^{-1}$ . The second Fourier coefficient ( $v_2$ ) of the azimuthal distribution of  $J/\psi$  is determined as a function of the transverse momentum ( $p_T$ ) using the event-plane method. The measurements were performed for several selections of collision centrality: 0%–50%, 10%–60%, and 10%–40%. We find that in all cases the values of  $v_2(p_T)$ , which quantify the elliptic flow of  $J/\psi$ , are consistent with zero. The results are consistent with measurements at midrapidity, indicating no significant elliptic flow of the  $J/\psi$  within the quark-gluon-plasma medium at collision energies of  $\sqrt{s_{NN}} = 200$  GeV.

## I. INTRODUCTION

A state of deconfined quarks and gluons, the quark-gluon plasma (QGP), is formed in heavy ion collisions at the BNL Relativistic Heavy Ion Collider (RHIC) [1–4]. The QGP has been found to exhibit a near-perfect-fluid behavior inferred from the strong correlations between the particles produced in the collisions [5]. These correlations are observed as an anisotropy in the final-state particle azimuthal distributions and are quantified by the components of the Fourier expansion of the invariant particle yields [6].

$$E \frac{d^3 N}{d^3 p} = \frac{1}{2\pi} \frac{d^2 N}{p_T dp_T dy} \left[ 1 + \sum_{n=1}^{\infty} 2v_n \cos[n(\phi - \Psi_n)] \right], \quad (1)$$

where  $\Psi_n$  represents the  $n^{\text{th}}$ -order symmetry plane angle, and  $v_n$  represent the flow coefficient for the  $n^{\text{th}}$ -harmonic. The second harmonic,  $v_2$ , known as “elliptic flow” is associated with the initial geometry of the overlap region of the colliding nuclei, which drives the anisotropy of the final-state particle distribution through anisotropic pressure gradients in the QGP.

Measuring the elliptic flow of heavy-flavor particles is of particular interest because due to their relatively large masses, the charm and beauty quarks may be thermodynamically distinct from the QGP medium. This feature,

in addition to their relatively long lifetimes and production in hard-scattering events during the initial stages of the collision, make them excellent probes for testing the properties of the QGP medium.

Previous measurements show a significant  $v_2$  of charmed hadrons in Au+Au collisions [7, 8] at RHIC, and of both charmed hadrons and charmonium bound states in Pb+Pb collisions [9–14] at the CERN Large Hadron Collider (LHC), indicating that even charm quarks diffuse in the QGP medium [15–21]. The production of the  $J/\psi$  meson, the most abundantly produced charmonium bound state, has been extensively studied at both RHIC [22–27] and the LHC [28–31]. However, the elliptic flow of the  $J/\psi$  at RHIC energies has remained inconclusive, due to the lack of statistical significance.

In relativistic heavy ion collisions, there are several mechanisms that may lead to azimuthal anisotropy in  $J/\psi$  production [32–36]. The produced  $J/\psi$  may be dissolved by the QGP, which creates anisotropies in the observed azimuthal distributions due to the different path lengths in the medium. If the charm quarks equilibrate within the medium, they may coalesce to form  $J/\psi$  which may acquire significant flow. Additionally, if the  $J/\psi$  mesons do not dissolve but thermalize inside the medium, they may follow the pressure gradients as lighter particles do.

Measurements of the nuclear modification ( $R_{AA}$ ) [37] of the production of  $J/\psi$  can provide insights on these competing mechanisms. The  $R_{AA}$  is defined as the ratio of the production in nucleus-nucleus (AA) collisions to the production in proton-proton collisions scaled to account for the number of binary nucleon collisions in the AA collisions. When comparing  $R_{AA}$  measurements at

\* Deceased

† PHENIX Spokesperson: akiba@rcf.rhic.bnl.gov

the LHC and RHIC [38], less suppression is observed at the LHC, contrary to expectations, as early theoretical calculations of  $J/\psi$  predicted that the suppression will become stronger as the QGP temperature increases [39]. Also unexpected, a greater  $J/\psi$  suppression is observed at forward rapidity than at midrapidity at RHIC [37]. The  $R_{AA}$  measurements can be explained [40] by models where  $J/\psi$  production has a contribution from coalescence of charm and anticharm quarks both at RHIC and the LHC. These contributions are more significant at the higher center-of-mass energy and at midrapidity, where more  $c\bar{c}$  pairs are produced. The same models support observations of a significant  $J/\psi$   $v_2$  at the LHC [9]. The RHIC measurement of  $J/\psi$   $v_2$  at midrapidity [41] appears to be consistent with zero, but has limited statistical significance. These measurements of  $J/\psi$   $v_2$  using the dimuon decay channel ( $J/\psi \rightarrow \mu^+ + \mu^-$ ) are the first at forward rapidity at RHIC.

## II. EXPERIMENTAL SETUP

Detailed below are the relevant detector subsystems of the PHENIX experiment [42], plus a discussion of the event and particle selections used in the analysis.

### A. PHENIX detectors

Figure 1 shows the PHENIX forward detectors (north and south arms) used in this analysis, which comprise the muon tracker (MuTr), muon identifier (MuID), forward-silicon-vertex detector (FVTX) and the beam-beam counter (BBC). The MuTr in each arm covers the pseudorapidity ranges of (north)  $1.2 < \eta < 2.4$  and (south)  $-2.2 < \eta < -1.2$  and comprises three octagonal stations of cathode-strip chambers. By measuring ionization produced within the gas-filled drift chambers, the MuTr reconstructs charged-particle trajectories, and subsequently measures their momenta. The MuID comprises five alternating layers of steel absorbers and Iarocci tubes. The successive hits in the Iarocci tubes form a “road” that is matched with MuTr tracks. The combined information from the MuTr and MuID is used to identify muons that form  $\mu^+\mu^-$  pairs to reconstruct the mesons  $J/\psi$  [43].

Two sets of detectors, FVTX and BBC, are used to reconstruct the second-order event plane  $\Psi_2$  with respect to which the  $J/\psi$  azimuthal anisotropy is measured. The FVTX is a four-layer silicon-strip detector placed perpendicular to the beam pipe at both sides of the collision point. The strips form 48 azimuthal segments covering the same rapidity range as the muon spectrometers. To avoid short-range correlations that are not associated with collective flow, the FVTX in the south arm is used to measure the flow of  $J/\psi$  in the north arm and vice versa. The BBCs that detect Čerenkov radiation comprise scintillators and photomultiplier tubes surrounding

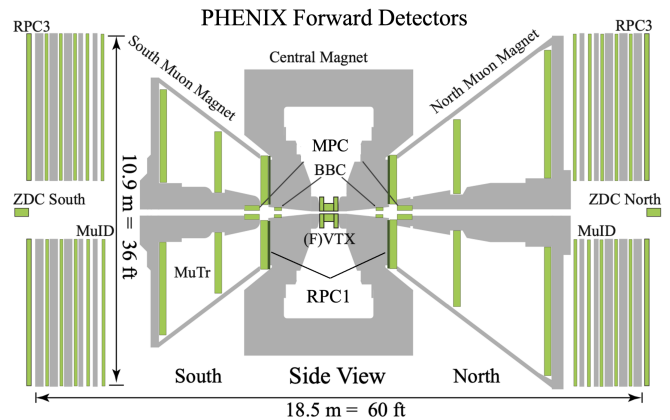


FIG. 1. A side view of the PHENIX muon-arm spectrometers.

the beam pipe and located between the muon arm and the central magnet [44]. The BBCs cover a pseudorapidity region of  $3.0 < |\eta| < 3.9$  and have full azimuthal coverage, providing multiplicity and centrality information, collision-vertex-position measurements, and reconstruction of the event plane.

The PHENIX central-arm tracking detectors (CNT) are drift chambers and pad chambers, which also are used for event-plane determination and are employed to determine the event-plane resolution as discussed in Section IIIB. Additionally, the central-arm silicon-vertex detector (VTX) [45] aids in accurately locating the primary-vertex point along the beam axis.

### B. Data samples and track selection

The integrated luminosity of the PHENIX 2014 and 2016 data sets are  $7.5 \text{ nb}^{-1}$  and  $7.0 \text{ nb}^{-1}$ , respectively, with a combined  $\approx 3.26 \times 10^{10}$  minimum-bias triggered events. A trigger system was employed to select collisions with a  $z$ -vertex within  $\pm 10$  cm from the center of the detector. Additionally, a dimuon trigger based on a combination of MuID hits selected a total of 380M dimuon candidates in the 2014 data set, and 307M in the 2016 data set.

Muons are identified by requiring that a detected particle penetrates several layers of absorber material in the MuID. By requiring the muon candidates to penetrate so far, hadron contribution is greatly reduced, although some hadrons may punch through. Particles that make it through this threshold, are then matched with the tracks reconstructed by the MuTr. Table I summarizes the track selections that are implemented to optimize the signal to background and were developed through detailed Monte-Carlo (MC) studies. The tracks in the MuTr must have a minimum of six hits and a  $\chi^2/\text{NDF}$  less than 10. The MuID roads must have at least three associated hits and MuID roads that have a  $\chi^2/\text{NDF}$  larger than 3 are rejected. The reconstructed muon tracks are

TABLE I. Summary of muon-track-selection criteria

Variable	Cut
$ y $	[1.2–2.2]
$p_T$	$\geq 1$ GeV/ $c$
$p_z$	$> 3$ GeV/ $c$
MuID penetration layer	3 or 4
Distance difference MuTr & MuID	$< 60$ mm·GeV/ $c$
Angular difference MuTr & MuID	$< 40$ mrad·GeV/ $c$
Track MuTr $\chi^2$	$< 10$
Track MuID $\chi^2$	$< 3$
# of MuTr track hits	$> 6$
# of MuID hits	$> 3$
Dimuon vertex refit $\chi^2$	$< 3$

required to have  $p_T > 1$  GeV/ $c$ , longitudinal momentum  $p_z > 3$  GeV/ $c$ , and track pseudorapidity within  $1.2 < |\eta| < 2.2$ .

Also applied are kinematic cuts to match the particle’s trajectory in the MuTr track and the MuID road. The distance between the MuTr track projection and the first MuID hit and the angle between the MuTr track projection and the MuID road linearly depend on the inverse of the particle momentum. The muon selection includes a maximum distance and angle between the MuTr track projections and MuID roads which are scaled by the muon candidate momentum as shown in Table I.

Muon pairs are refitted including the vertex position determined by the FVTX, and only pairs providing a refit with  $\chi^2 < 3$  are accepted. Additionally, dimuon pairs from decays of  $J/\psi$  with  $p_T < 5$  GeV/ $c$  are expected to produce tracks with opening angles larger than  $45^\circ$ . Therefore an opening angle cut is imposed to those dimuon pairs to reduce combinatorial background. Track selections are identical for both data sets and after implementation yield 210,389 dimuons in the 2014, and 140,587 in the 2016 data samples.

### III. DATA ANALYSIS

Detailed in this section are discussions of the extraction of the  $J/\psi$  yield, the measurement of azimuthal anisotropies, and the determination of systematic uncertainties

#### A. $J/\psi$ yield extraction

The  $J/\psi$  signal is obtained from the invariant-mass distribution of muon pairs near the expected  $J/\psi$  mass. The large contribution of random combinatorial background is estimated using opposite-charge muon pairs from different events. Mixed-event dimuon pairs are formed only if the two muons have differences less than 5% in cen-

trality, 0.75 cm in  $z$ -vertex, and  $\pi/20$  rad in event-plane angle. Otherwise, a mixed-event muon pair is not formed. The sample of mixed-event dimuons is about four times larger than dimuons from the same event. A normalization factor must be applied for the mixed-event sample, which can be obtained by using the ratio of like-sign pairs from the same event to like-sign pairs from mixed-events. The signal is then obtained by the subtraction of the normalized background from the foreground, which results in increased statistical precision when compared to the like-sign subtraction, and is of the form:

$$S = FG - N \cdot BG^{\text{mix}}, \quad (2)$$

where  $S$  is the signal,  $FG$  is the foreground distribution using opposite-sign muons from the same event,  $BG^{\text{mix}}$  is the background distribution created by mixing events, and  $N$  is the normalization factor that is obtained using:

$$N^{\text{mix}} = \frac{\sqrt{N_{\text{same}}^{++} \cdot N_{\text{same}}^{--}}}{\sqrt{N_{\text{mix}}^{++} \cdot N_{\text{mix}}^{--}}}, \quad (3)$$

where  $N^{++}$  and  $N^{--}$  denote the number of like-sign muon pairs, while “same” and “mix” denote whether the pair came from the same event or from event-mixing.  $N^{\text{mix}}$  is the resulting distribution, which has a mass dependence and was fit with a polynomial of degree two. The minimum of the function was taken to be  $N$  used to scale the combinatorial background,  $N = \min(N_{\text{mix}})$ . The uncertainty associated with the fit was determined to be 5% and is propagated as a systematic uncertainty. In the fitting of the mass distributions, the shape of the  $J/\psi$  signal is assumed to be a crystal-ball (CB) function [46], and the  $J/\psi$  count is obtained by the integral of the CB function in the fit (see Fig. 2).

#### B. Azimuthal anisotropy measurement

In a collision of two nuclei, the reaction plane is defined as the plane formed by the impact-parameter vector and the beam axis. In practice, because this reaction plane is not directly observable, the event-plane method is employed that uses the anisotropic flow itself to estimate the reaction-plane angle [6]. The  $x$  and  $y$  components of the event-flow vector  $Q_n$  and the event-plane angle  $\Psi_n$  are defined for each  $n^{\text{th}}$  harmonic by the following:

$$Q_x = \sum_{i=1}^N \omega_i \cos(n\phi_i), \quad (4)$$

$$Q_y = \sum_{i=1}^N \omega_i \sin(n\phi_i), \quad (5)$$

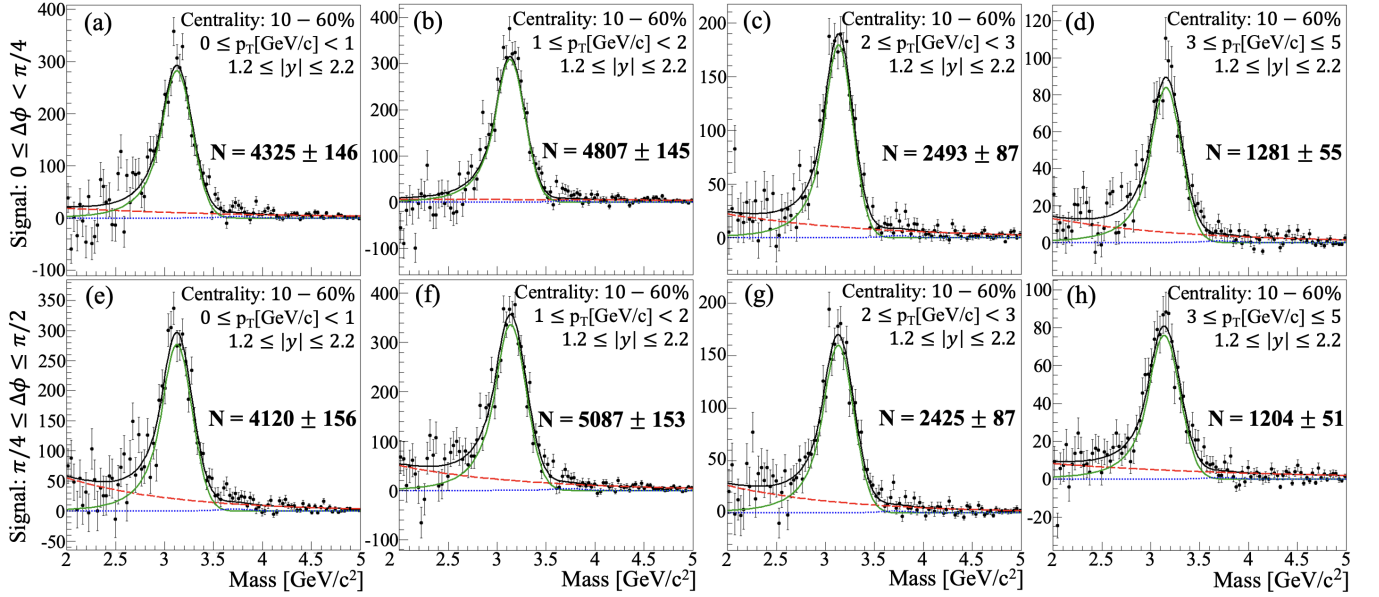


FIG. 2. Combined 2014 and 2016 data set dimuon invariant-mass distributions after mixed-event combinatorial background subtraction. The plots are binned by  $p_T$  in each column and in  $\Delta\phi$  for each row. In decreasing magnitude, the highest [black] curves are the total fits, the next highest [green] curves are CB fits to the  $J/\psi$  peak, the dashed [red] curves are exponential fits to the remaining background after combinatorial-background subtraction, and the dotted [blue] curves are CB fits to the  $\psi(2S)$  peak,

$$\Psi_n = \frac{1}{n} \tan^{-1} \left( \frac{Q_y}{Q_x} \right). \quad (6)$$

where the  $Q$ -vectors are measured by the sum of the vector components of the azimuthal angles ( $\phi$ ) of each particle  $i$  in an event, and  $\omega_i$  are weights that are set to 1. The observed  $v_n^{\text{obs}}$  with respect to the event plane is defined by:

$$v_n^{\text{obs}}(p_T, y) = \langle \cos[n(\phi_i - \Psi_n)] \rangle. \quad (7)$$

where  $\langle \rangle$  denotes an average over all particles and all events. The second-order event-plane angle  $\Psi_2$  used in measuring  $v_2$  is determined using the FVTX (south and north) detectors. The finite resolution in the detector and the finite number of particles used in event-plane determination require a resolution correction to  $v_2^{\text{obs}}$ :

$$v_2 = \frac{v_2^{\text{obs}}(p_T, y)}{\text{Res}(\Psi_2)}. \quad (8)$$

The associated event-plane resolutions (see Table II) are calculated using the standard three-subevent method [6], where the particles used in the event-plane determination are sorted in three regions A, B, C separated in pseudorapidity. Independent measurements are correlated using the FVTX, BBC, and CNT, for example:

$$\text{Res}(\Psi_2^A) = \sqrt{\frac{\langle \cos(2[\Psi_2^A - \Psi_2^B]) \rangle \langle \cos(2[\Psi_2^A - \Psi_2^C]) \rangle}{\langle \cos(2[\Psi_2^B - \Psi_2^C]) \rangle}} \quad (9)$$

where the  $\Psi_2^A$  is the second-harmonic event plane measured with the FVTX (either south or north),  $\Psi_2^B$  is from the BBC (opposite arm north or south), and  $\Psi_2^C$  is from the CNT.

To measure  $v_2^{\text{obs}}$  the foreground and background dimuons are split into two bins of  $\Delta\phi = (\phi_i - \Psi_2)$ , where dimuons from  $\Delta\phi = [-\pi/4, \pi/4]$  are considered to be “in-plane” with the event plane, and dimuons from  $\Delta\phi = [-\pi/2, -\pi/4]$  and  $[\pi/4, \pi/2]$  are “out-of-plane.” The  $J/\psi$  signals are reconstructed for both sets to obtain the yield (See Table III), and then the  $J/\psi$  yields are fit as a function of  $\Delta\phi$  with the following equation:

$$f(\Delta\phi) = N_0(1 + 2v_2^{\text{obs}} \cos(2\Delta\phi)), \quad (10)$$

where  $N_0$  is a normalization factor, and  $v_2^{\text{obs}}$  is the free-elliptic-flow parameter. After extracting  $v_2^{\text{obs}}$  for each data set, the event-plane resolution is corrected. A weighted average between the 2014 and 2016 datasets is obtained using the statistical uncertainties of the two measurements as weights. Repeating this for each measurement evaluates the systematic uncertainties.

### C. Systematic uncertainties

Below are detailed descriptions of the sources of systematic uncertainty.

TABLE II. Event-plane resolutions using the FVTX as the primary event-plane detector.

Centrality	$Res(\Psi_2^{\text{FVTX}})$	$Res(\Psi_2^{\text{BBC}})$
0%–10%	0.3035	0.1833
10%–20%	0.5359	0.2637
20%–30%	0.5701	0.2803
30%–40%	0.5391	0.2582
40%–50%	0.4639	0.2108
50%–60%	0.3620	0.1546

TABLE III. The  $J/\psi$  yields recorded in 2014 and 2016 within the in-plane (in) and out-of-plane (out)  $\Delta\phi$  bins.

Year	$p_T$ bin (GeV/c)	$N_{\text{in}}$	$N_{\text{out}}$
2014	0.0–1.0	$2727 \pm 100$	$2454 \pm 107$
	1.0–2.0	$2863 \pm 145$	$3136 \pm 110$
	2.0–3.0	$1636 \pm 65$	$1456 \pm 63$
	3.0–5.0	$791 \pm 42$	$780 \pm 38$
2016	0.0–0.5	$832 \pm 65$	$770 \pm 72$
	0.5–1.0	$1872 \pm 82$	$1648 \pm 87$
	1.0–5.0	$5415 \pm 146$	$5373 \pm 127$
	0.0–5.0	$8189 \pm 160$	$7845 \pm 164$
	0.0–1.0	$1498 \pm 125$	$1685 \pm 88$
	1.0–2.0	$1930 \pm 79$	$1985 \pm 95$
	2.0–3.0	$937 \pm 54$	$970 \pm 51$
	3.0–5.0	$493 \pm 32$	$438 \pm 31$
	0.0–0.5	$470 \pm 50$	$643 \pm 50$
	0.5–1.0	$1025 \pm 81$	$1026 \pm 75$
1.0–5.0	$3399 \pm 100$	$3398 \pm 109$	
0.0–5.0	$4965 \pm 131$	$5092 \pm 136$	

### 1. Background contributions

The like-sign method is an alternative to estimate the combinatorial background. The background is created using dimuon pairs of the same sign ( $\mu^+\mu^+$  and  $\mu^-\mu^-$ ) that come from the same event:

$$BG = 2R\sqrt{N^{++}N^{--}}, \quad (11)$$

where  $N^{++}$  and  $N^{--}$  are the like-sign dimuon counts per mass bin, and  $R$  is a normalization factor that is obtained by taking a ratio of the foreground over background in a region where a signal ( $M_{\mu\mu} = [1.5\text{--}2.5]$  GeV/ $c^2$ ) is not expected. The contribution to the final systematic uncertainty is small, indicating good agreement between the

two background-estimation methods.

Because the measurement using mixed-event BG estimation has smaller uncertainties in the final  $v_2$  measurement, the default is chosen to be mixed-event subtraction. The uncertainty of the mixed-event background normalization was determined to be  $\pm 5\%$ . This is propagated to the final systematic uncertainty by varying the normalization by  $\pm 5\%$ , reconstructing the  $J/\psi$  for these two sets of mass distributions, and calculating the resulting  $v_2$  for each set.

### 2. Track selections

To evaluate the uncertainty from the track selections listed in Table I, the selections were varied to make them tighter or looser by 10% and the analysis was performed to obtain  $v_2$  as in the default measurement. Table IV shows the maximum absolute difference in  $v_2$  measured in each  $p_T$  and centrality interval.

### 3. Detector effects

The  $J/\psi$  efficiency is not uniform across the measured  $p_T$  and rapidity ranges and if the  $v_2$  signal is nonzero or has a  $p_T$  and rapidity dependence within the measured bins, the  $v_2$  measurements will be distorted. These distortions were evaluated in simulations and propagated as systematic uncertainties. A sample of  $J/\psi$  decays were simulated and reconstructed with a full GEANT4 [47] detector simulation. The  $J/\psi$  sample was weighted according to the yield measured by PHENIX [24]. The event-plane angle was set to 0 and the  $J/\psi$  azimuthal angle distributions was modulated according to:

$$f(\phi) = 1 + 2v_2^{\text{gen}}(p_T, \eta, \text{centrality}) \cos(2\phi), \quad (12)$$

where  $v_2^{\text{gen}}$  are the  $v_2$  measured by the CMS [13, 48] and ALICE [9] detectors at the LHC. The LHC measurements are used to estimate an upper limit for our  $J/\psi$   $v_2$  signal. The difference between the measured  $v_2$  of reconstructed  $J/\psi$  from this sample and  $v_2^{\text{gen}}$  is no larger than 0.002, which is included in the systematic uncertainty.

### 4. Fourier fitting

The uncertainties associated with the coarse binning in the  $\Delta\phi$  distributions are used to obtain the  $v_2$  values. As a systematic check, the  $J/\psi$  yields are split into three  $|\Delta\phi|$  bins ( $[0-\pi/6]$ ,  $[\pi/6-\pi/3]$ , and  $[\pi/3-\pi/2]$ ) and are fit to the  $|\Delta\phi|$  distributions with Eq. 10. After extracting  $v_2^{\text{obs}}$  for each data set, the event-plane resolutions are corrected. The absolute difference between the  $v_2$  values obtained with two or three  $\Delta\phi$  bins are taken as a systematic uncertainty and listed in Table IV as  $\Delta\phi$  Bin.



### 5. Event-plane detector

In the standard analysis the  $J/\psi$  mesons detected in the south (north) muon spectrometer are correlated with the event plane determined in the FTVX from the opposite arm, north (south). The selection imposes a pseudorapidity gap of  $2.4 < |\Delta\eta| < 4.4$  between the particles used in the flow analysis and those used to determine the event-plane angle. As a systematic check, the event-plane angle determined in the north (south) FVTX is replaced with the angle measured in BBC north (south). The resulting  $v_2^{\text{obs}}$  measurement is corrected with the BBC event-plane resolution. The absolute difference between the two  $v_2$  measurements is propagated as a systematic uncertainty.

### 6. Summary of systematic uncertainties

Table IV presents the contributions of each of the systematic uncertainties for  $J/\psi$   $v_2$  as a function of  $p_T$  in the PHENIX muon arms ( $1.2 < |\eta| < 2.2$ ) for the centrality selections 10%–60%, 0%–50%, and 10%–40%. The descriptions for each contribution are:

**LSS:** The contribution from using like-sign background subtraction

**$N^{\text{mix}}$ :** The contribution from altering the mixed-event normalization by the associated uncertainty of determining the normalization factor

**Track Selection:** The contribution from altering the track quality cuts from Table I by 10% of their default values

**EFF:** The contribution from nonuniform detector acceptance

**$\Delta\phi$  Bin:** The contribution from the selection of  $\Delta\phi$  binning in the Fourier fits

**EP:** The contribution from the event-plane detector selection

**Total:** The total systematic uncertainty of the contributions, which are assumed to be independent, for each  $p_T$  bin and added in quadrature

## IV. RESULTS AND DISCUSSION

In the first centrality range (10%–60%) of Table IV, the  $v_2$  was measured for three configurations of  $p_T$  (see Fig. 3 and Fig. 4): (1) standard binning ([0.0–1.0], [1.0–2.0], [2.0–3.0], and [3.0–5.0] GeV/c), (2) special binning ([0.0–0.5], [0.5–1.0], and [1.0–5.0] GeV/c), and (3) with one inclusive  $p_T$  bin ([0.0–5.0] GeV/c). In each case, the measured  $J/\psi$   $v_2$  is consistent with zero within uncertainties, and the numerical values are shown in Table V.

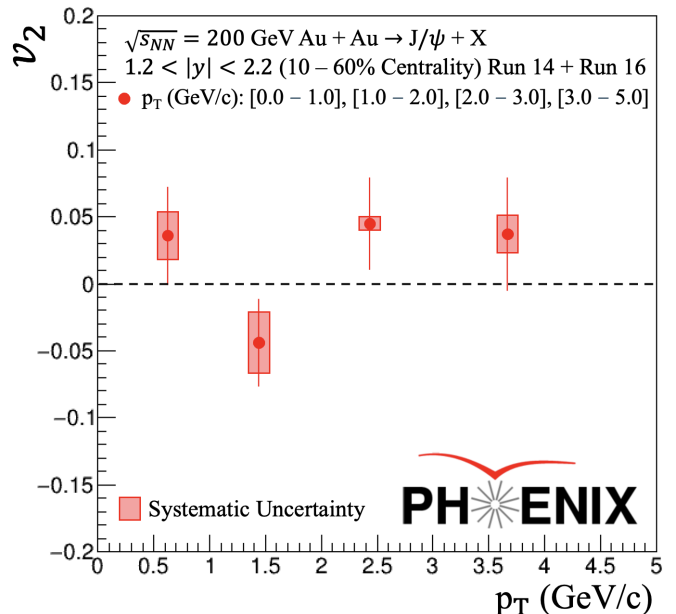


FIG. 3. Measurement of  $J/\psi$   $v_2$  at forward rapidity ( $1.2 < |\eta| < 2.2$ ) for centrality 10%–60% in Au+Au collisions at  $\sqrt{s_{NN}} = 200$  GeV. The measurements are performed for the  $p_T$  selections [0.0–1.0], [1.0–2.0], [2.0–3.0], and [3.0–5.0] GeV/c. The data points are plotted at the mean  $p_T$  for each bin.

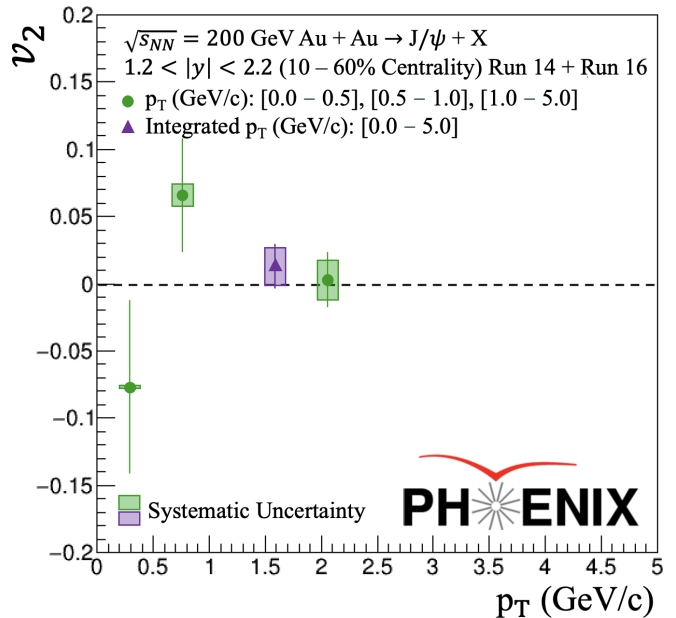


FIG. 4. Measurement of  $v_2$  of  $J/\psi$  at forward rapidity ( $1.2 < |\eta| < 2.2$ ) for centrality 10%–60% in Au+Au collisions at  $\sqrt{s_{NN}} = 200$  GeV. The solid circle [green] data points are measurements for the  $p_T$  selections [0.0–0.5], [0.5–1.0], and [1.0–5.0] GeV/c. The triangle [dark blue] data point at  $p_T = 1.6$  GeV/c is for the integrated  $p_T$  selection [0.0–5.0] GeV/c. All data points are plotted at the mean  $p_T$  for each bin.



TABLE IV. Summary of systematic uncertainty contributions for centralities 10%–60%, 10%–40%, and 0%–50%. See text for descriptions of each contribution.

Centrality	$p_T(\text{GeV}/c)$	LSS	$\mathbf{N}^{\text{mix}}$	Track Selection	EFF	$\Delta\phi$ Bin	EP	Total
10%–60%	0.0–1.0	0.0133	0.0107	0.0025	0.0020	0.0022	0.0038	0.018
	1.0–2.0	0.0051	0.0172	0.0091	0.0020	0.0114	0.0015	0.023
	2.0–3.0	0.0015	0.0006	0.0019	0.0020	0.0046	0.0005	0.005
	3.0–5.0	0.0042	0.0003	0.0022	0.0020	0.0081	0.0102	0.014
10%–40%	0.0–0.5	0.0004	0.0003	0.0005	0.0020	0.0004	0.0001	0.001
	0.5–1.0	0.0061	0.0018	0.0012	0.0020	0.0012	0.0049	0.008
	1.0–5.0	0.0019	0.0078	0.0040	0.0020	0.0120	0.0011	0.015
	0.0–5.0	0.0059	0.0085	0.0045	0.0020	0.0082	0.0013	0.014
10%–40%	0.0–2.0	0.0214	0.0145	0.0058	0.0020	0.0105	0.0052	0.029
	2.0–5.0	0.0265	0.0003	0.0128	0.0020	0.0055	0.0002	0.025
	5.0–10.0	0.0178	0.0006	0.0263	0.0020	0.0056	0.0677	0.075
0%–50%	0.0–2.0	0.0116	0.0149	0.0214	0.0020	0.0015	0.0144	0.032
	2.0–5.0	0.0084	0.0000	0.0032	0.0020	0.0006	0.0064	0.011
	5.0–10.0	0.0142	0.0004	0.0216	0.0020	0.0079	0.0591	0.065

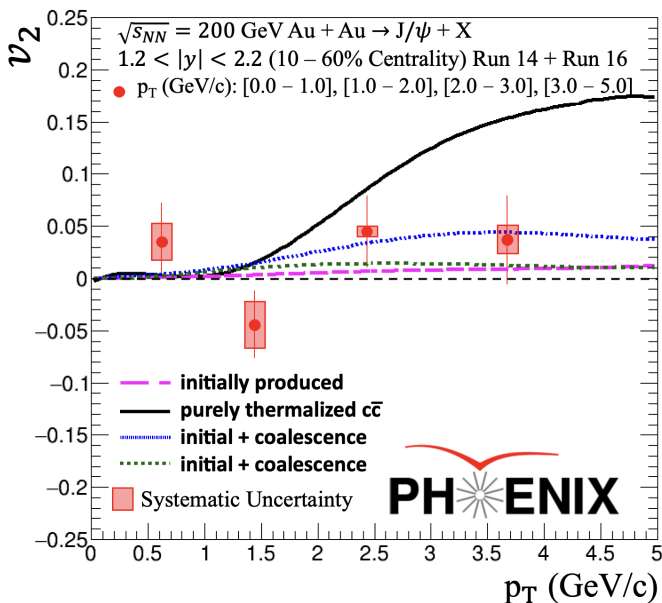


FIG. 5. Forward-rapidity  $J/\psi$   $v_2$  as a function of  $p_T$  for centrality 10%–60% in Au+Au collisions at  $\sqrt{s_{NN}} = 200$  GeV compared to various theoretical models [33–36]. The mean  $p_T$  for each bin is used for each measurement.

Figure 5 compares the PHENIX measurement of  $J/\psi$  elliptic flow at forward rapidity to several theoretical models [33–36] that were previously compared to the STAR measurement of  $J/\psi$   $v_2$  at midrapidity [41]. The  $J/\psi$  production mechanisms vary for each of these mod-

els, with the “initially produced” and “coalescence from thermalized  $c\bar{c}$ ” models being at the opposite ends of the spectrum. In the initially-produced model [33],  $J/\psi$  mesons are produced in the initial hard scattering without the consideration of regeneration in the QGP. In this case azimuthal anisotropy can be generated through path-length-dependent dissociation of  $J/\psi$  in the medium. This effect appears to be small.

As an upper limit of the  $J/\psi$  flow, the authors of ref. [34] consider the production of  $J/\psi$  from coalescence of thermalized  $c$  and  $\bar{c}$  at hadronization, where the quark elliptic flow is fully developed. Alternatively [33], the  $c$  and  $\bar{c}$  coalescence can be considered throughout the QGP evolution which will allow for charmonium creation at earlier stages when the quark flow is smaller.

In a realistic scenario, both initial production and coalescence must be included. Two-component models that consider the interplay of both mechanisms were employed in refs. [35, 36]. In both cases coalescence plays a significant role in  $J/\psi$  production at low- $p_T$ , and the higher  $p_T$  ( $\approx 2$  GeV/ $c$ ) is dominated by perturbative quantum chromodynamics. In contrast, the flow of the charm quarks is boosted to higher  $p_T$  than that of the light quarks due to radial flow leading to overall near-zero elliptic flow for  $J/\psi$  with  $p_T < 1$  GeV/ $c$ . Combining the two mechanisms leads to nonzero  $v_2$  of  $J/\psi$  at higher  $p_T$  peaking around  $p_T \approx 3$  GeV/ $c$ , but the magnitude is small. In the scenario where  $c\bar{c}$  coalescence happens at hadronization [35] the  $v_2$  of  $J/\psi$  reaches up to 3%, but is smaller in the case of continuous coalescence [36]. Our data exclude a scenario in which  $J/\psi$  are produced entirely from coales-

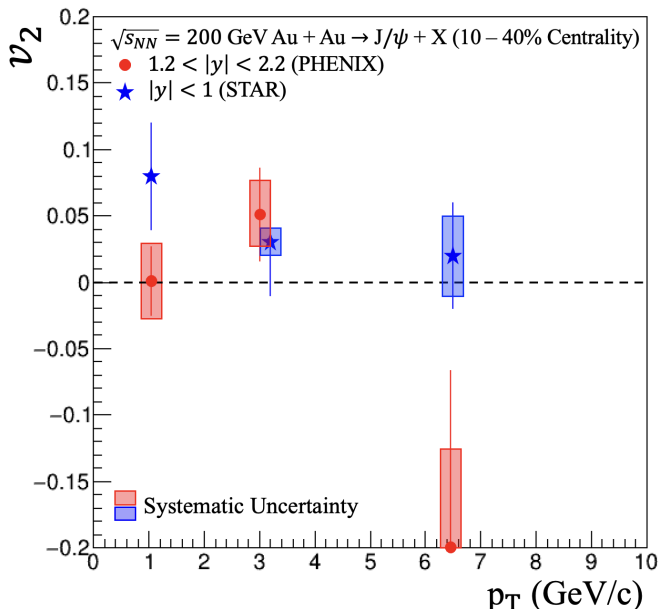


FIG. 6. Comparison of measurements between PHENIX (round [red] data points) at forward rapidity and STAR [41] (star-symbol [blue] data points) at midrapidity for  $J/\psi$   $v_2$  as a function of  $p_T$  for centrality 10%–40% in Au+Au collisions at  $\sqrt{s_{NN}} = 200$  GeV. The  $p_T$  bins for both measurements are [0.0–2.0], [2.0–5.0], and [5.0–10.0] GeV/c, and all data are plotted at the mean  $p_T$  for each bin.

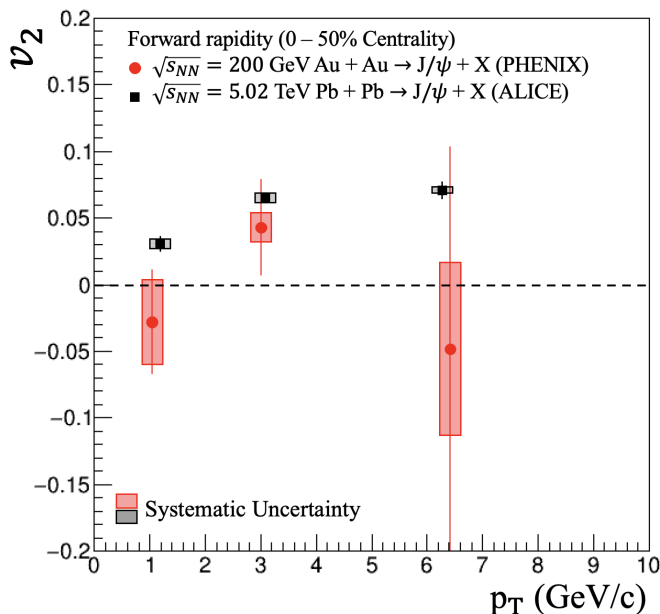


FIG. 7. The  $J/\psi$   $v_2$  as a function of  $p_T$  for centrality 0%–50% at forward rapidity. The circle [red] data points are for PHENIX Au+Au collisions at  $\sqrt{s_{NN}} = 200$  GeV for  $1.2 < |y| < 2.2$  and the square [black] data points are for ALICE Pb+Pb collisions at  $\sqrt{s_{NN}} = 5.02$  TeV for  $2.4 < |y| < 4$  [9]. The  $p_T$  bins for both measurements are [0.0–2.0], [2.0–5.0], and [5.0–10.0] GeV/c. The data points are plotted at the mean  $p_T$  for each bin.

TABLE V. Values of  $J/\psi$   $v_2$  measured in the 10%–60%, 10%–40%, and 0%–50% centrality ranges with statistical and systematic uncertainties. The 10%–40% and 0%–50% centrality ranges are used to facilitate comparisons with previous measurements by STAR [41] (See Fig.6) and ALICE [9] (See Fig.7), respectively.

$\langle p_T \rangle$ [GeV/c]	$J/\psi$ $v_2$	Measurement
10%–60%	0.62	$0.036 \pm 0.036^{\text{stat}} \pm 0.018^{\text{sys}}$
	1.44	$-0.044 \pm 0.032^{\text{stat}} \pm 0.023^{\text{sys}}$
	2.43	$0.045 \pm 0.034^{\text{stat}} \pm 0.005^{\text{sys}}$
	3.67	$0.037 \pm 0.042^{\text{stat}} \pm 0.014^{\text{sys}}$
10%–40%	0.30	$-0.077 \pm 0.064^{\text{stat}} \pm 0.001^{\text{sys}}$
	0.76	$0.066 \pm 0.042^{\text{stat}} \pm 0.008^{\text{sys}}$
	2.06	$0.003 \pm 0.020^{\text{stat}} \pm 0.015^{\text{sys}}$
	6.45	$-0.201 \pm 0.133^{\text{stat}} \pm 0.075^{\text{sys}}$
0%–50%	1.59	$0.013 \pm 0.016^{\text{stat}} \pm 0.014^{\text{sys}}$
	3.00	$0.043 \pm 0.036^{\text{stat}} \pm 0.011^{\text{sys}}$
	6.41	$-0.048 \pm 0.151^{\text{stat}} \pm 0.065^{\text{sys}}$

cence of thermalized charm quarks. However, the models cannot be distinguished from each other when including only primordial  $J/\psi$  or production through coalescence.

To facilitate direct comparisons to previous measurements of  $J/\psi$  elliptic flow at RHIC and the LHC, measurements are performed for other centrality and  $p_T$  selections ([0.0–2.0], [2.0–5.0], and [5.0–10.0] GeV/c). Figure 6 compares, in the centrality range of 10%–40%, this PHENIX measurement at forward rapidity with the STAR midrapidity result [41]. A significant rapidity dependence or significant elliptic flow of  $J/\psi$  is not observed in Au+Au collisions at  $\sqrt{s_{NN}} = 200$  GeV. Figure 7 compares the PHENIX and ALICE results [9], where both measurements are performed at forward rapidity and in the centrality range of 0%–50%. The PHENIX measurement is systematically lower than the  $v_2$  values observed by ALICE. Note that the PHENIX measurements are consistent with zero elliptic flow, while there is a clear signal in the LHC measurements. The numeric values of  $v_2$  used in the comparisons with previous measurements are shown in Table V.

## V. SUMMARY AND CONCLUSIONS

In summary, elliptic-flow measurements of inclusive  $J/\psi$  production are presented as a function of  $p_T$  at forward rapidity ( $1.2 \leq |y| \leq 2.2$ ) in Au+Au collisions at  $\sqrt{s_{NN}} = 200$  GeV. The  $J/\psi$  mesons were reconstructed in

$\mu^+\mu^-$  decay channel using the PHENIX muon-arm spectrometers. The  $v_2$  measurements were performed with the event-plane method. The event plane was determined using the north and south FVTX detectors in the opposite muon arm (south or north) where the  $J/\psi$  was measured. The PHENIX Au+Au data sets collected in 2014 and 2016 sampled integrated luminosity of  $14.5 \text{ nb}^{-1}$ . The measurements were performed for several centrality selections (10%–60%, 10%–40%, and 0%–50%) and compared both to theoretical models and to earlier measurements for midrapidity at RHIC and for forward rapidity at the LHC.

In conclusion, The PHENIX measurements at forward rapidity are consistent with zero, which is similar to the midrapidity measurement from STAR. This is distinct from the ALICE results at the LHC, which support significant  $J/\psi$  production through charm-quark coalescence. The PHENIX data exclude a large contribution at RHIC energies to  $J/\psi$  production and flow at forward rapidity from coalescence of thermalized  $c\bar{c}$  quarks.

### ACKNOWLEDGMENTS

We thank the staff of the Collider-Accelerator and Physics Departments at Brookhaven National Laboratory and the staff of the other PHENIX participating institutions for their vital contributions. We acknowledge support from the Office of Nuclear Physics in the

Office of Science of the Department of Energy, the National Science Foundation, Abilene Christian University Research Council, Research Foundation of SUNY, and Dean of the College of Arts and Sciences, Vanderbilt University (U.S.A), Ministry of Education, Culture, Sports, Science, and Technology and the Japan Society for the Promotion of Science (Japan), Natural Science Foundation of China (People's Republic of China), Croatian Science Foundation and Ministry of Science and Education (Croatia), Ministry of Education, Youth and Sports (Czech Republic), Centre National de la Recherche Scientifique, Commissariat à l'Énergie Atomique, and Institut National de Physique Nucléaire et de Physique des Particules (France), J. Bolyai Research Scholarship, EFOP, HUN-REN ATOMKI, NKFIH, and OTKA (Hungary), Department of Atomic Energy and Department of Science and Technology (India), Israel Science Foundation (Israel), Basic Science Research and SRC(CENuM) Programs through NRF funded by the Ministry of Education and the Ministry of Science and ICT (Korea). Ministry of Education and Science, Russian Academy of Sciences, Federal Agency of Atomic Energy (Russia), VR and Wallenberg Foundation (Sweden), University of Zambia, the Government of the Republic of Zambia (Zambia), the U.S. Civilian Research and Development Foundation for the Independent States of the Former Soviet Union, the Hungarian American Enterprise Scholarship Fund, the US-Hungarian Fulbright Foundation, and the US-Israel Binational Science Foundation.

- 
- [1] K. Adcox *et al.* (PHENIX Collaboration), Formation of dense partonic matter in relativistic nucleus-nucleus collisions at RHIC: Experimental evaluation by the PHENIX collaboration, *Nucl. Phys. A* **757**, 184 (2005).
- [2] I. Arsene *et al.* (BRAHMS Collaboration), Quark gluon plasma and color glass condensate at RHIC? The Perspective from the BRAHMS experiment, *Nucl. Phys. A* **757**, 1 (2005).
- [3] B. B. Back *et al.* (PHOBOS Collaboration), The PHOBOS perspective on discoveries at RHIC, *Nucl. Phys. A* **757**, 28 (2005).
- [4] J. Adams *et al.* (STAR Collaboration), Experimental and theoretical challenges in the search for the quark gluon plasma: The STAR Collaboration's critical assessment of the evidence from RHIC collisions, *Nucl. Phys. A* **757**, 102 (2005).
- [5] U. W. Heinz, The Strongly coupled quark-gluon plasma created at RHIC, *J. Phys. A* **42**, 214003 (2009).
- [6] A. M. Poskanzer and S. A. Voloshin, Methods for analyzing anisotropic flow in relativistic nuclear collisions, *Phys. Rev. C* **58**, 1671 (1998).
- [7] T. Hachiyu *et al.* (PHENIX Collaboration), Nuclear modification factor and flow of charm and bottom quarks in Au+Au collisions at  $\sqrt{s_{NN}} = 200\text{GeV}$  by the PHENIX Experiment, *Nucl. Phys. A* **982**, 663 (2019).
- [8] L. Adamczyk *et al.* (STAR Collaboration), Measurement of  $D^0$  Azimuthal Anisotropy at Midrapidity in Au+Au Collisions at  $\sqrt{s_{NN}}=200 \text{ GeV}$ , *Phys. Rev. Lett.* **118**, 212301 (2017).
- [9] S. Acharya *et al.* (ALICE Collaboration),  $J/\psi$  elliptic and triangular flow in Pb-Pb collisions at  $\sqrt{s_{NN}} = 5.02 \text{ TeV}$ , *J. High Energy Phys.* **10** (2020), 141.
- [10] M. Aaboud *et al.* (ATLAS Collaboration), Prompt and non-prompt  $J/\psi$  elliptic flow in Pb+Pb collisions at  $\sqrt{s_{NN}} = 5.02 \text{ TeV}$  with the ATLAS detector, *Eur. Phys. J. C* **78**, 784 (2018).
- [11] A. Tumasyan *et al.* (CMS Collaboration), Measurements of the azimuthal anisotropy of prompt and nonprompt charmonia in PbPb collisions at  $\sqrt{s_{NN}} = 5.02 \text{ TeV}$ , *J. High Energy Phys.* **10** (2023), 115.
- [12] V. Khachatryan *et al.* (CMS Collaboration), Suppression and azimuthal anisotropy of prompt and nonprompt  $J/\psi$  production in PbPb collisions at  $\sqrt{s_{NN}} = 2.76 \text{ TeV}$ , *Eur. Phys. J. C* **77**, 252 (2017).
- [13] A. M. Sirunyan *et al.* (CMS Collaboration), Measurement of prompt  $D^0$  meson azimuthal anisotropy in Pb-Pb collisions at  $\sqrt{s_{NN}} = 5.02 \text{ TeV}$ , *Phys. Rev. Lett.* **120**, 202301 (2018).
- [14] A. Tumasyan *et al.* (CMS Collaboration), Probing Charm Quark Dynamics via Multiparticle Correlations in Pb-Pb Collisions at  $\sqrt{s_{NN}} = 5.02 \text{ TeV}$ , *Phys. Rev. Lett.* **129**, 022001 (2022).
- [15] M. Nahrgang, J. Aichelin, P. B. Gossiaux, and K. Werner, Influence of hadronic bound states above  $T_c$  on heavy-

- quark observables in Pb + Pb collisions at the CERN Large Hadron Collider, *Phys. Rev. C* **89**, 014905 (2014).
- [16] M. He and R. Rapp, Hadronization and Charm-Hadron Ratios in Heavy-Ion Collisions, *Phys. Rev. Lett.* **124**, 042301 (2020).
- [17] S. Cao, G.-Y. Qin, and S. A. Bass, Energy loss, hadronization and hadronic interactions of heavy flavors in relativistic heavy-ion collisions, *Phys. Rev. C* **92**, 024907 (2015).
- [18] T. Song, H. Berrehrah, D. Cabrera, J. M. Torres-Rincon, L. Tolos, W. Cassing, and E. Bratkovskaya, Tomography of the Quark-Gluon-Plasma by Charm Quarks, *Phys. Rev. C* **92**, 014910 (2015).
- [19] W. Ke, Y. Xu, and S. A. Bass, Modified Boltzmann approach for modeling the splitting vertices induced by the hot QCD medium in the deep Landau-Pomeranchuk-Migdal region, *Phys. Rev. C* **100**, 064911 (2019).
- [20] S. Li and J. Liao, Data-driven extraction of heavy quark diffusion in quark-gluon plasma, *Eur. Phys. J. C* **80**, 671 (2020).
- [21] S. Plumari, G. Coci, V. Minissale, S. K. Das, Y. Sun, and V. Greco, Heavy- light flavor correlations of anisotropic flows at LHC energies within event-by-event transport approach, *Phys. Lett. B* **805**, 135460 (2020).
- [22] A. Adare *et al.* (PHENIX Collaboration),  $J/\psi$  Production in  $\sqrt{s_{NN}} = 200$  GeV Cu+Cu Collisions, *Phys. Rev. Lett.* **101**, 122301 (2008).
- [23] U. A. Acharya *et al.* (PHENIX Collaboration),  $J/\psi$  and  $\psi(2S)$  production at forward rapidity in  $p+p$  collisions at  $\sqrt{s} = 510$  GeV, *Phys. Rev. D* **101**, 052006 (2020).
- [24] A. Adare *et al.* (PHENIX Collaboration),  $J/\psi$  Production vs Centrality, Transverse Momentum, and Rapidity in Au+Au Collisions at  $\sqrt{s_{NN}}=200$  GeV, *Phys. Rev. Lett.* **98**, 232301 (2007).
- [25] A. Adare *et al.* (PHENIX Collaboration),  $J/\psi$  production versus transverse momentum and rapidity in  $p^+p$  collisions at  $\sqrt{s} = 200$  GeV, *Phys. Rev. Lett.* **98**, 232002 (2007).
- [26] J. Adam *et al.* (STAR Collaboration),  $J/\psi$  production cross section and its dependence on charged-particle multiplicity in  $p+p$  collisions at  $\sqrt{s} = 200$  GeV, *Phys. Lett. B* **786**, 87 (2018).
- [27] L. Adamczyk *et al.* (STAR Collaboration),  $J/\psi$  production at high transverse momenta in  $p+p$  and Au+Au collisions at  $\sqrt{s_{NN}}=200$  GeV, *Phys. Lett. B* **722**, 55 (2013).
- [28] S. Acharya *et al.* (ALICE Collaboration), Measurements of inclusive  $J/\psi$  production at midrapidity and forward rapidity in Pb–Pb collisions at  $s_{NN} = 5.02$  TeV, *Phys. Lett. B* **849**, 138451 (2024).
- [29] S. Acharya *et al.* (ALICE Collaboration), Prompt and non-prompt  $J/\psi$  production at midrapidity in Pb–Pb collisions at  $\sqrt{s_{NN}} = 5.02$  TeV, *J. High Energy Phys.* **02** (2024), 066.
- [30] S. Acharya *et al.* (ALICE Collaboration), Inclusive quarkonium production in  $pp$  collisions at  $\sqrt{s} = 5.02$  TeV, *Eur. Phys. J. C* **83**, 61 (2023).
- [31] A. M. Sirunyan *et al.* (CMS Collaboration), Measurement of quarkonium production cross sections in  $pp$  collisions at  $\sqrt{s} = 13$  TeV, *Phys. Lett. B* **780**, 251 (2018).
- [32] X. Yao and B. Müller, Quarkonium inside the quark-gluon plasma: Diffusion, dissociation, recombination, and energy loss, *Phys. Rev. D* **100**, 014008 (2019).
- [33] L. Yan, P. Zhuang, and N. Xu, Competition between  $J/\psi$  suppression and regeneration in quark-gluon plasma, *Phys. Rev. Lett.* **97**, 232301 (2006).
- [34] V. Greco, C. M. Ko, and R. Rapp, Quark coalescence for charmed mesons in ultrarelativistic heavy ion collisions, *Phys. Lett. B* **595**, 202 (2004).
- [35] X. Zhao and R. Rapp, Charmonium Production at High  $p(t)$  at RHIC, in *24th Winter Workshop on Nuclear Dynamics* (2008) arXiv:0806.1239.
- [36] Y. Liu, N. Xu, and P. Zhuang,  $J/\psi$  elliptic flow in relativistic heavy ion collisions, *Nucl. Phys. A* **834**, 317C (2010).
- [37] A. Adare *et al.* (PHENIX Collaboration),  $J/\psi$  suppression at forward rapidity in Au+Au collisions at  $\sqrt{s_{NN}}=200$  GeV, *Phys. Rev. C* **84**, 054912 (2011).
- [38] J. Adam *et al.* (ALICE Collaboration),  $J/\psi$  suppression at forward rapidity in Pb-Pb collisions at  $\sqrt{s_{NN}} = 5.02$  TeV, *Phys. Lett. B* **766**, 212 (2017).
- [39] T. Matsui and H. Satz,  $J/\psi$  Suppression by Quark-Gluon Plasma Formation, *Phys. Lett. B* **178**, 416 (1986).
- [40] K. Zhou, N. Xu, Z. Xu, and P. Zhuang, Medium effects on charmonium production at ultrarelativistic energies available at the CERN Large Hadron Collider, *Phys. Rev. C* **89**, 054911 (2014).
- [41] L. Adamczyk *et al.* (STAR Collaboration), Measurement of  $J/\psi$  Azimuthal Anisotropy in Au+Au Collisions at  $\sqrt{s_{NN}} = 200$  GeV, *Phys. Rev. Lett.* **111**, 052301 (2013).
- [42] K. Adcox *et al.* (PHENIX Collaboration), PHENIX detector overview, *Nucl. Instrum. Methods Phys. Res., Sec. A* **499**, 469 (2003).
- [43] H. Akikawa *et al.* (PHENIX Collaboration), PHENIX muon arms, *Nucl. Instrum. Methods Phys. Res., Sec. A* **499**, 537 (2003).
- [44] T. Nakamura, Phenix focus: Beam beam counter (2020).
- [45] R. Nouicer (PHENIX Collaboration), PHENIX Upgrade: Novel Stripixel Detector for Heavy Quark Detection and Proton Spin Structure Measurements at RHIC Energies, *Nucl. Instrum. Methods Phys. Res., Sec. B* **261**, 1067 (2007).
- [46] J. E. Gaiser, *Charmonium Spectroscopy From Radiative Decays of the  $J/\psi$  and  $\psi'$* , Master's thesis, Stanford University (1982).
- [47] S. Agostinelli *et al.* (GEANT4 Collaboration), GEANT4—a simulation toolkit, *Nucl. Instrum. Methods Phys. Res., Sec. A* **506**, 250 (2003).
- [48] A. M. Sirunyan *et al.* (CMS Collaboration), Azimuthal anisotropy of charged particles with transverse momentum up to 100 GeV/  $c$  in PbPb collisions at  $\sqrt{s_{NN}}=5.02$  TeV, *Phys. Lett. B* **776**, 195 (2018).